Available online at www.sciencedirect.com
ScienceDirect
JOURNAL OF RARE EARTHS, Vol. 30, No. 11, Nov. 2012, P. 1177
JOURNAL OF RARE EARTHS
www.re-journal.com/en/

Effect of rare-earth oxides on properties of silicon nitride obtained by normal sintering and sinter-HIP

Cecilia C. Guedes-Silva[1], Flávio Machado de Souza Carvalho[2], José Carlos Bressiani[1]

(1.Nuclear and Energy Research Institute - IPEN/CNEN, 2242 Prof. Lineu Prestes Avenue, São Paulo, SP, 05508-000, Brazil; 2. Geoscience Institute - IGC/USP, 562 Lago Street, São Paulo, SP, 05508-080, Brazil)

Received 19 March 2012; revised 27 August 2012

Abstract: This paper presented the microstructure, mechanical properties and oxidation behavior of silicon nitride obtained by both conventional sintering and sintering followed by hot isostatic pressing (HIP). Silicon nitride with additives such as 5 wt.% Al_2O_3 and 5 wt.% Ln_2O_3 (Ln= La, La concentrate, Gd or La+Gd) were studied. The results revealed that Gd_2O_3 additions increased the formation of elongated grains of β-Si_3N_4, the fracture toughness and oxidation resistance. La_2O_3 additions led to higher densification and hardness values, while addition of La_2O_3 concentrate promoted the formation of materials with intermediate properties, compared to the other studied compositions. Hot isostatic pressing increased the hardness but decreased the fracture toughness of the material, mainly because it allowed residual pores to close and also reduced the average aspect ratio of β-Si_3N_4 grains.

Keywords: rare earths; silicon nitride properties; normal sintering; sinter-HIP

Silicon nitride (Si_3N_4) ceramics have been extensively investigated owing to their potential use as structural material in a wide temperature range. This is mainly due to their chemical stability, superior wear resistance, high hardness and strength. Since 1955, researches have shown that silicon nitride has good thermal and chemical stability in metal baths. This enabled its development for use as thermocouples coating and crucible for melting metals. Nevertheless, interest in this material continued to grow, mainly for use in gas turbine components to improve fuel burn efficiency, lower gases emissions and reduced levels of particulates[1]. Other features of silicon nitride such as low density, low inertia and high wear resistance allowed its use in conventional internal combustion and adiabatic diesel engines[2].

Because it is a covalent ceramic and has a high vapor pressure at high temperatures, it is very difficult to densify silicon nitride by solid state diffusion mechanisms, requiring additives that promote liquid phase sintering[3]. The sintering additives react with the silica layer on the Si_3N_4 powder surface, forming a liquid phase in which the α-Si_3N_4 dissolves and re-precipitates as β-Si_3N_4. It is extremely important to understand the role of sintering aids on the microstructure of the material because the liquid phase remains at the grain boundaries as an amorphous or secondary crystalline phase after cooling and this has a marked influence on the final properties of the material[4–6].

Hence, the type and amount of sintering additives determine the temperature for onset of densification, the rate at which sintering occurs, the morphology of β-Si_3N_4 grains and the characteristics of the phase at the grain boundary. Among the various additives that have been used, rare-earth oxides are prominent since they control some steps of the sintering process and features of the final microstructure, e.g. α→β phase transformation rates and aspect ratio of β-Si_3N_4 grains[4]. As a consequence, properties such as fracture toughness, hardness and wear as well as oxidation resistance tend to improve with the addition of rare-earth oxides to silicon nitride ceramics.

A number of studies about the influence of rare-earth oxides as sintering aids of silicon nitride were performed in 80′s, 90′s and 00′s. Among these, Sanders et al.[7] investigated the effect of adding SiO_2 together with Y_2O_3, CeO_2, La_2O_3 or Sm_2O_3 on the microstructure and mechanical properties of silicon nitride. They found that additions of Y_2O_3 promoted the formation of more elongated grains of β-Si_3N_4, and increased bend strength from room temperature up to 1000 ºC. Hot pressed silicon nitride disilicate ceramics with oxides of Y, Yb, Ho, Dy, Er, Sm, Ce, Lu, La, Pr, and Gd were studied by Choi et al.[8]. These authors associated the cation radius of the oxide additives with high temperature properties and noted that both the flexural strength at 1200 ºC and oxidation resistance at 1400 ºC increased with decrease in cation radius. In 2002, Hong et al.[9] also fabricated silicon nitride disilicate ceramics ($RE_2Si_2O_7$; RE=Nd, Sm, Y, Yb) by hot pressing followed by annealing at 1450 ºC for 4 h. Their results demonstrated that the rare-earth oxides affect the densification process and the shrinkage temperature. They also reported increased high temperature strength of ceramics which contained $Yb_2Si_2O_7$ and $Y_2Si_2O_7$.

This paper presented and discussed the microstructure,

Corresponding author: Cecilia C. Guedes-Silva (**E-mail:** cecilia.guedes@ipen.br; **Tel.:** +55-11-3133-9304)

DOI: 10.1016/S1002-0721(12)60201-4

mechanical properties and oxidation behavior of silicon nitride ceramics containing additions of alumina together with La_2O_3, Gd_2O_3, a mixture of La_2O_3 and Gd_2O_3, as well as La_2O_3 concentrate. These ceramics were prepared by conventional sintering and sintering followed hot isostatic pressing (HIP). Considering the applications of structural materials at temperatures as high as 1400 ºC, the oxidation behavior of the ceramics was evaluated at this temperature at various time intervals up to 64 h of exposure.

1 Materials and methods

The starting materials were powders of Si_3N_4 (M11, Hermann; with 92.7 wt.% α-Si_3N_4 and 1.14 wt.% oxygen), Gd_2O_3 (CDTN; purity > 99.9 %), La_2O_3 (Sigma; purity> 99.9%), La_2O_3 concentrate (IPEN; 75.6 wt.% La) and α-Al_2O_3 (16 SG Alcoa; purity>99.9%). The chemical composition of the La_2O_3 concentrate, as determined by X-ray fluorescence analysis is shown in Table 1.

To obtain the samples, mixtures with different compositions as shown in Table 2 were ground in an atrittor mill using isopropanol as liquid vehicle. The ground and homogenized powder mixtures were dried at 90 ºC, uniaxially compacted at 50 MPa and cold isostatically pressed at 200 MPa.

Dilatometry measurements were carried out with a dilatometer (Netzsch DIL 402 E/7) to determine the densification behavior and to select the optimum thermal cycle prior to sintering in a carbon resistance furnace. In the dilatometer, the samples were heated to 1750 ºC at 20 ºC/min and held for 60 min in a nitrogen atmosphere.

Conventional sintering of the samples was carried out in a carbon resistance furnace (Nukem GMBH 645) in nitrogen atmosphere under conditions similar to those used in the dilatometer studies, i.e., 1750 ºC for 60 min. A powder bed of silicon nitride was prepared to avoid evaporation of the oxide and decomposition of the silicon nitride.

Sinter-HIP process was also used in the samples and was characterized by hot isostatically pressing (HIP) at 1700 ºC for 30 min after the conventional sintering. The sinter-HIPed samples were designated as SN-GH, SN-LH, SN-LCH and SN-LGH.

The bulk density of the samples was measured using the Archimedes displacement method and the theoretical density was calculated according to the mixtures rule. X-ray powder diffraction analysis (X-ray powder diffractometer with Cu-Kα radiation, Siemens D5000) and examination by scanning electron microscopy (SEM, Jeol-JXA 6400) were performed in the samples to identify the crystalline phases and to observe the shape and grain size as well as its distribution. The average aspect ratio of the grains was determined from the SEM micrographs using an imaging analyzer (Leco-2001).

The hardness and indentation fracture toughness (K_{IC}) at room temperature were determined using a Vickers diamond indenter and a 50 N load (Durometer, Amsler Otto Wolpert-Werke GMBH). The fracture toughness was determined by the Anstis[10] method assuming a value of 300 GPa[11] for Young's modulus.

The oxidation measurements were carried out using 2 mm× 5 mm×4 mm wide sinter-HIPed specimens that were wet polished with SiC abrasive paper up to 600 grit and ultrasonically cleaned with acetone. The oxidation tests were carried out at 1400 ºC for 64 h in a tube furnace (Bloomfield) and the weight gain measured after 1, 2, 4, 8, 16, 32 and 64 h of exposure, with an analytical balance with an accuracy of ±0.001 mg.

The oxidized layer on the specimens were examined by scanning electron microscopy (SEM, Jeol-JXA 6400) to determine the morphology of the phases that were present and the crystalline phases were identified using X-ray powder diffraction analysis (X-ray powder diffractometer with Cu-Kα radiation, Siemens D5000).

Table 1 Rare-earth cation content in the La_2O_3 concentrate powder (wt.%)

Elements	Pr	Nd	Ce	Gd	Tb
Contents	17.27	3.22	1.92	1.36	0.47

Table 2 Composition of the different silicon nitride ceramics

Designation	Composition
SN-G	Si_3N_4+5.0 wt.% Al_2O_3+5.0 wt.% Gd_2O_3
SN-L	Si_3N_4+5.0 wt.% Al_2O_3+5.0 wt.% La_2O_3
SN-LC	Si_3N_4+5.0 wt.% Al_2O_3+5.0 wt.% La_2O_3 Concentrate (LC)
SN-LG	Si_3N_4+5.0 wt.% Al_2O_3+2.5 wt.% La_2O_3+2.5 wt.% Gd_2O_3

2 Results and discussion

2.1 Densification behavior and microstructure development

Plots obtained by dilatometer and registered during investigations are shown in Fig. 1 and these reveal the changes in dimension of the different samples. The starting point for shrinkage is characterized by liquid formation and the temperature at which this happens is shown in Table 3. This leads to particle rearrangement, which is the first stage of the liquid sintering process.

The data shown in Fig. 1 and Table 3 indicate that shrinkage of the samples started at temperatures as low as 1200 ºC. Additionally, the data reveal that densification of samples containing La_2O_3 and Al_2O_3 initiated at temperatures lower than that of the samples containing Gd_2O_3 and Al_2O_3. The SN-LG sample had lower shrinkage onset temperature compared to the SN-G sample, but higher than that of the SN-L sample. The shrinkage onset temperature of the sample containing La_2O_3 concentrate (SN-LC) was higher than that of the samples containing only pure La_2O_3 and Al_2O_3 (SN-L).

The cation radius of the oxide additives may have contributed to variation in the shrinkage onset temperature. Rare-earth cations with large radius (La^{3+} with r_i=117.2 pm)

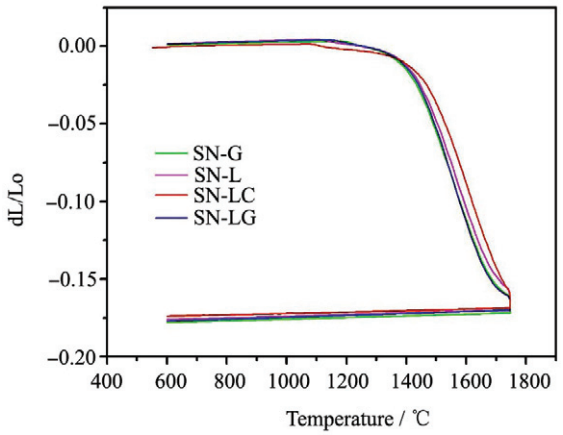

Fig. 1 Densification curves of silicon nitride samples with different compositions

Table 3 Liquid formation temperature of the silicon nitride samples determined from the densification curves

Composition	SN-G	SN-L	SN-LC	SN-LG
T/ºC	1200	1100	1150	1180

seemed to reduce the liquid formation temperature, while cations with smaller radius like Gd^{3+} (r_i=108.8 pm) in SN-G and SN-LG, Pr^{3+} (r_i=113 pm), Ce^{3+} (r_i=115 pm) and Tb^{3+} (r_i=106 pm) in SN-LC (see Table 1) increased this temperature.

Table 4 shows that silicon nitride samples with high densities can be obtained by the conventional sintering process, i.e., without application of pressure. On the basis of this table, it can be noted that addition of Gd_2O_3 in SN-G and SN-LG lowered the final density compared to addition of only La_2O_3 (SN-L samples). The same behavior was noted when La_2O_3 concentrate was used (SN-LC samples) as the additive in the place of pure La_2O_3, suggesting that higher La_2O_3 contents led to increase in the final density, for the sintering conditions used in this investigation.

Sintering followed by HIP gave samples with densities higher than 98% TD (theoretical density). However, a lower final density value of only 95% TD was obtained for the SN-GH sample (Table 4), indicating that there were residual closed pores even after HIP.

Table 4 Microstructure features and mechanical properties of silicon nitride samples obtained by conventional sintering and sintering followed by hot isostatic pressing (sinter-HIP)

Compositions	ρ/(%TD)	Aspect ratio of β-Si_3N_4 grains	H_v/ GPa	K_{IC}/ (MP·$m^{1/2}$)
Samples obtained by conventional sintering				
SN-G	93	2.9±0.8	11.7±0.5	5.1±0.7
SN-L	97	2.4±0.7	13.7±0.5	4.6±0.6
SN-LC	97	2.8±0.6	13.8±0.6	5.0±0.7
SN-LG	95	3.0±0.8	13.1±0.2	4.8±0.6
Sinter-HIPed samples				
SN-GH	95	1.9±0.6	13.0±0.3	4.4±0.5
SN-LH	98	2.1±0.8	14.6±0.4	3.9±0.3
SN-LCH	99	1.9±0.6	15.1±0.4	4.2±0.5
SN-LGH	98	1.7±0.5	15.6±0.3	4.1±0.4

Based on the X-ray powder diffraction spectra (XRPD) shown in Figs. 2 and 3, it can be observed that complete α→ β-Si_3N_4 transformation (JCPDS pattern No. 01-033-1160) was achieved in the conventional sintering process. β-Si_3N_4 remained as an exclusive crystalline phase in the materials, except in SN-G sample, whose XRPD spectra (Fig. 2) suggests that gadolinium oxide (Gd_2O_3, hexagonal, JCPDS card No. 00-043-1014) and quartz low (SiO_2, hexagonal, JCPDS card No. 01-070-2538) are present at its grain boundaries. Nonetheless, it can be speculated that these phases may have dissolved in the residual intergranular phase when the sample was submitted by HIP treatment (Fig. 3).

Fig. 4 shows the microstructures of etched surfaces of the samples sintered at 1750 ºC for 1 h. These micrographs reveal the homogeneous microstructure characterized by elongated β-Si_3N_4 grains (as indicated in Fig. 2) with similar aspect ratios (Table 4). After HIP, the average aspect ratios of β-Si_3N_4 grains decreased (Table 4 and microstructures in Fig. 5), and this was more pronounced in samples with initial high aspect ratio grains.

In contrast, no significant differences were observed among the microstructures of sinter-HIPed samples (Fig. 5), which is also in agreement with the aspect ratio results

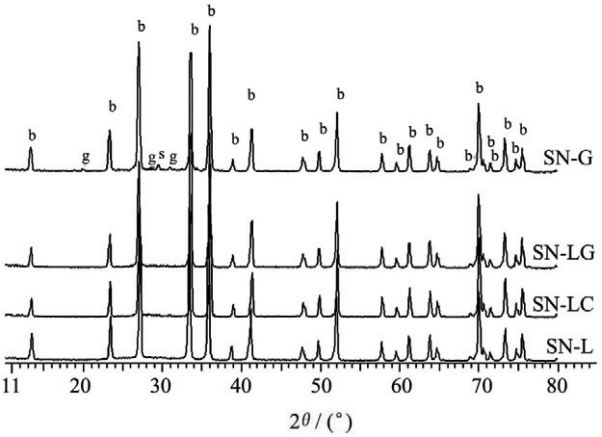

Fig. 2 X-ray diffraction (XRD) spectra of conventionally sintered silicon nitride samples (b is β-Si_3N_4, g is Gd_2O_3 and s is quartz low)

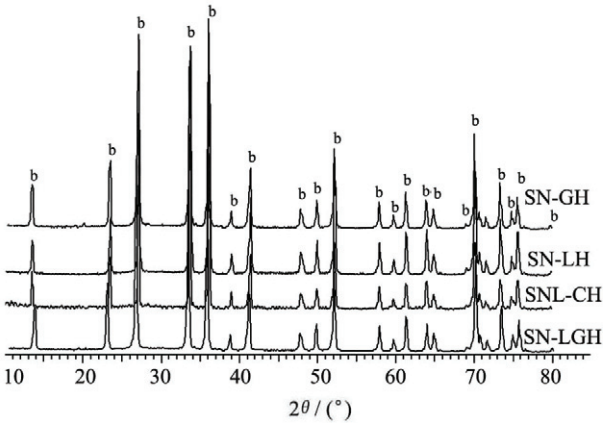

Fig. 3 X-ray diffraction (XRD) spectra of silicon nitride samples that were sintered and hot isostatically pressed (b is β-Si_3N_4)

shown in Table 4.

2.2 Mechanical properties

The Vickers hardness (H_V) and fracture toughness (K_{IC}) of the samples are given in Table 4 along with their densities. It is apparent that the hardness is directly related to ceramic processing and to porosity of the samples. The increase in density of the samples confirms elimination of the closed pores in most of the sinter-HIPed samples, with maximum increase of 2.5 GPa for the SN-LGH sample compared to the SN-LG sample.

Except SN-GH, the hardness of the samples were affected mainly by the low initial density and the addition of La_2O_3 concentrate. Samples with Gd_2O_3 were harder than those

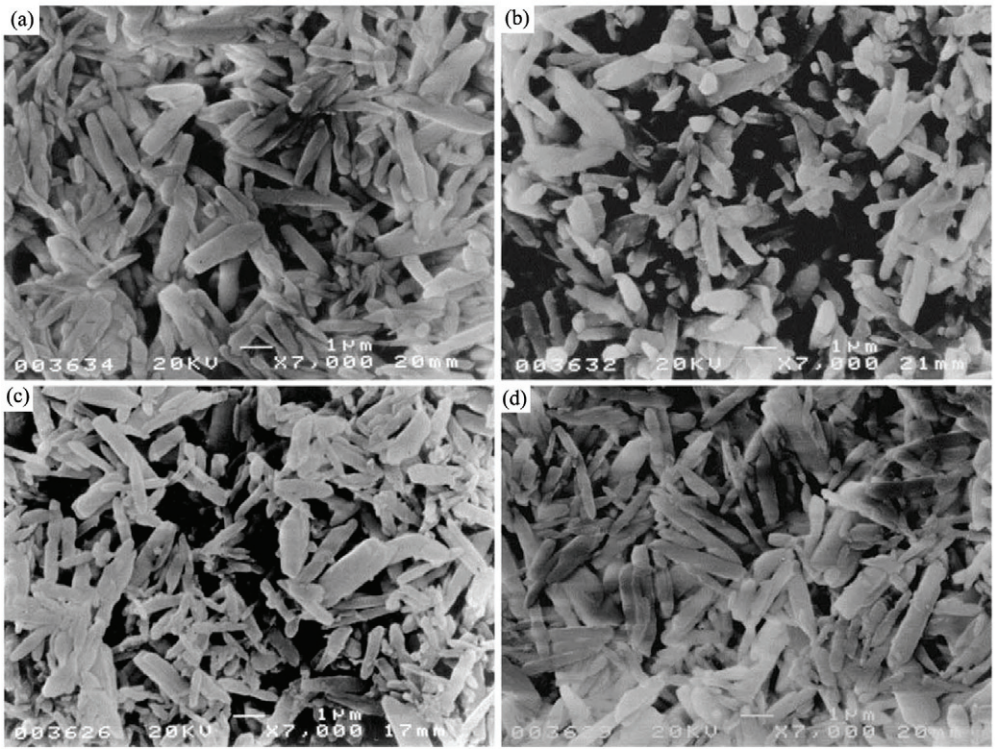

Fig. 4 Scanning electron micrographs of conventionally sintered sample surfaces that were polished and then etched with NaOH (These micrographs reveal elongated grains of β-Si_3N_4)

(a) SN-G; (b) SN-L; (c) SN-LC; (d) SN-LG

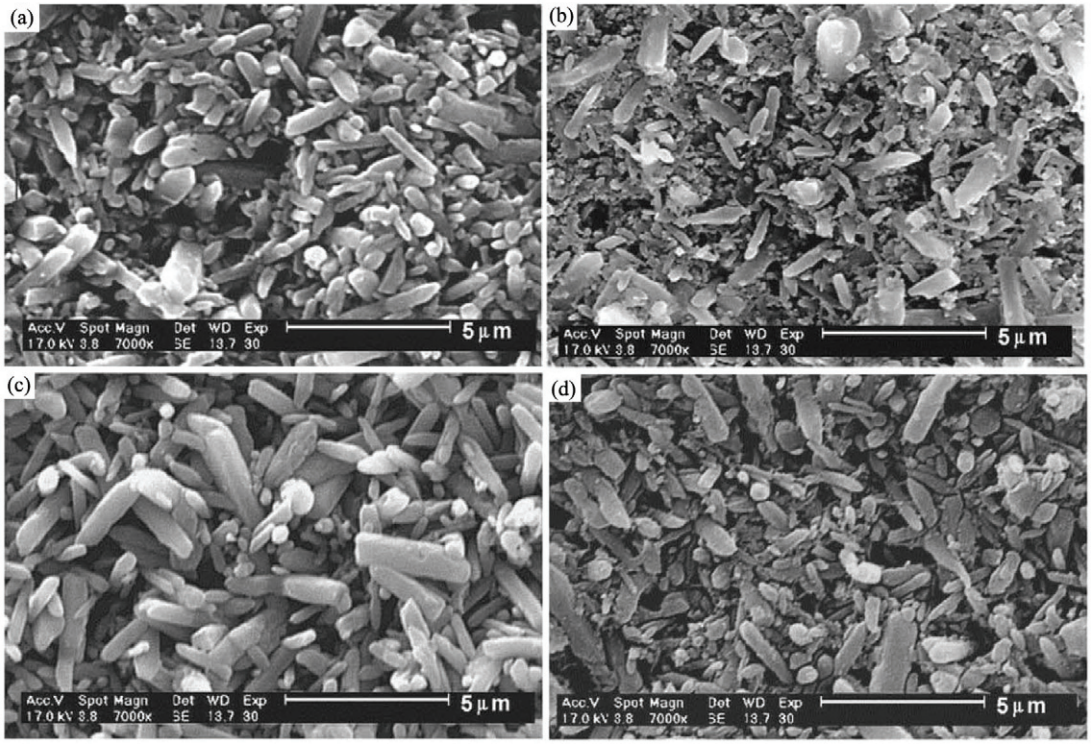

Fig. 5 Scanning electron micrographs of polished sinter-HIPed samples surfaces etched with NaOH

(a) SN-GH; (b) SN-LH; (c) SN-LCH; (d) SN-LGH

with pure La_2O_3. These results can be attributed to the intergranular phase that tends to be more resistant and more viscous in the presence of small rare-earth cations[12].

Further analysis of data in Table 4, indicates that samples obtained by conventional sintering attained K_{Ic} values within the expected range and over 4 MPa·m$^{1/2}$. Meanwhile, variation in fracture toughness values can be linked to the properties of the secondary phase of specific samples. The SN-LC, SN-LG and SN-G samples obtained by conventional sintering had higher fracture toughness than those containing only La_2O_3 and Al_2O_3 (SN-L sample) as additives. This behavior can be attributed to microstructure changes, characterized by more elongated grains, which gives rise to phenomena such as crack deflection, crack bridging and grain pullout.

Further, a decrease in fracture toughness of the sinter-HIPed samples was noted because of rounding of grains promoted by heat treatment at temperature above that of liquid formation[13]. This can be observed by comparing the microstructures shown in Fig. 5 with those in Fig. 4.

2.3 Oxidation behavior

Fig. 6 shows variation of specific mass gain as a function of time of silicon nitride samples at 1400 ºC. The oxidation behavior indicates that it obeys a parabolic rate law (Eq. (1)), suggesting that the oxidation kinetics are controlled by diffusion. The formula in Eq. (1) has been used in many studies describing oxidation kinetics of silicon nitride ceramics[14,15].

$$(\Delta m/A)^2=kt \quad (1)$$

Where Δm is the mass gain, A is area, k is the rate constant and t is the exposure time. The rate constants of the different samples, as determined from the curves in Fig. 6, are shown in Table 5 and those with lower rate constants exhibited higher oxidation resistance. The rate constants in the range 1.01×10^{-4} to 2.82×10^{-4} g/(cm^2·h$^{1/2}$) are similar to those reported by Pomeroy and Hampshire[16], for silicon nitride ceramics with additions of magnesia and neodymia, but exposed to 1300 ºC for 26 h. These results demonstrate the good oxidation behavior of the samples that were studied, as the temperature (1400 ºC) was higher and the exposure time (64 h) was longer than those used by the above mentioned authors.

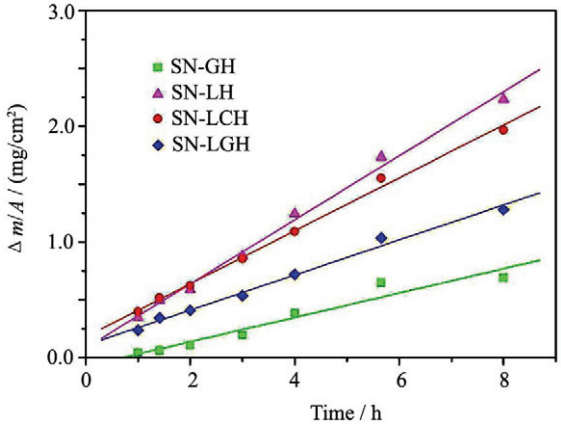

Fig. 6 Plots of mass gain versus exposure time of the different samples at 1400 ºC in air

Table 5 Rate constants and mass gain of sinter-HIPed samples exposed to air for 64 h at 1400 ºC

Samples	k/(10^{-4} g/(cm^2·h$^{1/2}$))	$\Delta m/A$/(mg/cm^2)
SN-GH	1.01	0.69
SN-LH	2.82	2.24
SN-LCH	2.40	1.97
SN-LGH	1.58	1.27

It can be observed from Fig. 6, Tables 4 and 5 that even with density lower than that of other samples, the SN-GH sample had the lowest mass gain (0.69 mg/cm^2) and rate constant (1.01×10^{-4} g/(cm^2·h$^{1/2}$)). This was followed by SN-LGH, SN-LCH and SN-LH with progressively increasing mass gains. This indicates that with addition of Gd_2O_3 along with Al_2O_3, the silicon nitride ceramic had higher oxidation resistance compared to those with La_2O_3 and Al_2O_3. Moreover, the mass gain results (Table 5) are consistent with the values obtained by Pan[17] and by Echeberria and Castro[18]. The former reported 0.8 mg/cm^2 for silicon nitride ceramics doped with 21 vol.% Y_2O_3/SiO_2 and exposed to air for 64 h at 1400 ºC and the latter reported 2.23 mg/cm^2 for samples with additions of CeO_2 and Al_2O_3 and exposure to 1400 ºC for only 20 h.

The differences in oxidation behavior could be attributed to formation of phases during the sintering step and subsequent cooling. Since the initial microstructures, i.e., crystalline phases, grain size and shape of the samples are similar (Table 4 and Figs. 3 and 5), the highest oxidation resistance of the Gd_2O_3 containing sample can be linked to the viscosity of silicate glasses. Viscous silicate glasses as the secondary phase are considered to inhibit oxygen migration[19]. Additionally, Gd^{3+} cations are more stable than La^{3+} in the intergranular phase reducing its migration from the grain boundaries to the surface. This indicates that addition of any other rare-earth cation, alone or with La^{3+} (as with SN-LCH and SN-GH), will result in material with higher oxidation resistance.

XRPD spectra shown in Fig. 7 indicate that besides β-Si_3N_4, α-cristobalite and rare-earth disilicates are present on the surfaces of oxidized specimens. Further, the diffraction

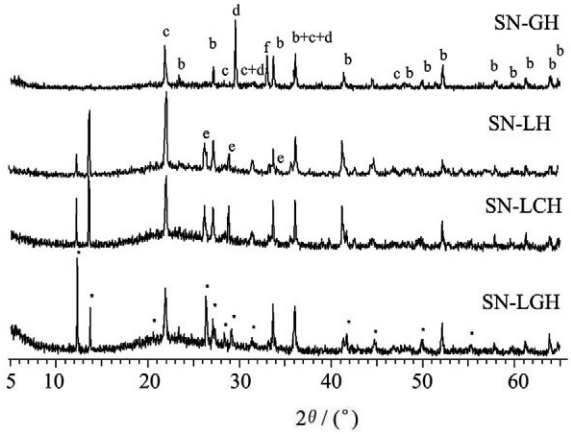

Fig. 7 X-ray diffraction (XRD) spectra of oxidized silicon nitride surfaces after 64 h of exposure at 1400 ºC (b is β-Si_3N_4, c is cristobalite, d is $Gd_2Si_2O_7$, e is $La_2Si_2O_7$ and * is $Ln_2Si_2O_5$)

patterns are dominated by a broad band that covers 2θ angle range between 15º and 30º, characteristic of amorphous silica. A layer of silica glass must have formed on sample surfaces during the oxidation tests due to oxygen diffusion, but partial crystallization as α-cristobalite probably occured during the cooling stage.

Lanthanum disilicate ($La_2Si_2O_7$, monoclinic, JCPDS card 01-081-0461) and gadolinium disilicate ($Gd_2Si_2O_7$, triclinic, JCPDS card 01-074-3570) were found on SN-LH, SN-LCH and SN-GH surfaces, respectively, as a result of rare-earth cation migration from the intergranular phase of silicon nitride to the surface. Besides cristobalite, the oxidation of SN-LGH sample also led to formation of other crystalline phases with the same structure as that of $Nd_2Si_2O_7$ (orthorhombic, JCPDS card 00-38-1456), but identification of its exact composition from the current XRPD database was not possible. As reported earlier[20], Eu^{3+}, Sm^{3+}, Nd^{3+} and La^{3+} ions formed isostructural disilicates (JCPDS card 01-38-1456), which lead us to establish that this compound was a $La_2Si_2O_7$ polymorph, designated by asterisks and $Ln_2Si_2O_7$ as a generic formula (Fig. 7). This assumption was based on the initial composition of SN-LGH sample which contained only Gd^{3+} and La^{3+} as the rare-earth ions.

Examination of the XRPD spectra reveals clearly that crystallization of $La_2Si_2O_7$ was favoured compared to $Gd_2Si_2O_7$, even when both lanthanum and gadolinium oxides were added together. This can be attributed to the higher rate of diffusion of La^{3+} compared to Gd^{3+}, through the intergranular phase and justifies the lower oxidation resistance of the samples containing higher amounts of La_2O_3, as shown in Fig. 6 and Table 5.

Fig. 8 shows that the oxide layers consisted of crystals and this depended on the composition of the sample. While there were elongated crystals on the SN-GH sample, the oxidized surface of SN-LH contained a large amount of crystals with small aspect ratio. On SN-LCH sample, the crystals were smaller but with morphology quite similar to those found on the SN-GH sample, considering even the formation of disilicate with different crystalline structures and previously identified by XRPD.

Further, cracks were found on the oxidized surfaces (see arrows in Fig. 8) caused by the difference in thermal expansion coefficient between the substrate and the oxide layer as well as the volume change due to transformation of the glassy phase to a crystalline phase during the cooling process.

3 Conclusions

The results have shown that small amounts of Gd_2O_3 and/or La_2O_3 along with Al_2O_3 were sufficient to produce dense ceramics with elongated β-Si_3N_4 grains. However, samples prepared by conventional sintering required higher amounts of La_2O_3 for it to have higher density and hardness, but it had lower fracture toughness. These additions also resulted in the microstructure being composed of β-Si_3N_4 grains with the smallest aspect ratio. An opposite behavior was observed in samples containing higher amounts of Gd_2O_3 that led to formation of materials with lower density and hardness, but with higher fracture toughness.

The use of La_2O_3 concentrate as a sintering aid gave samples with density as high as that of the sample containing

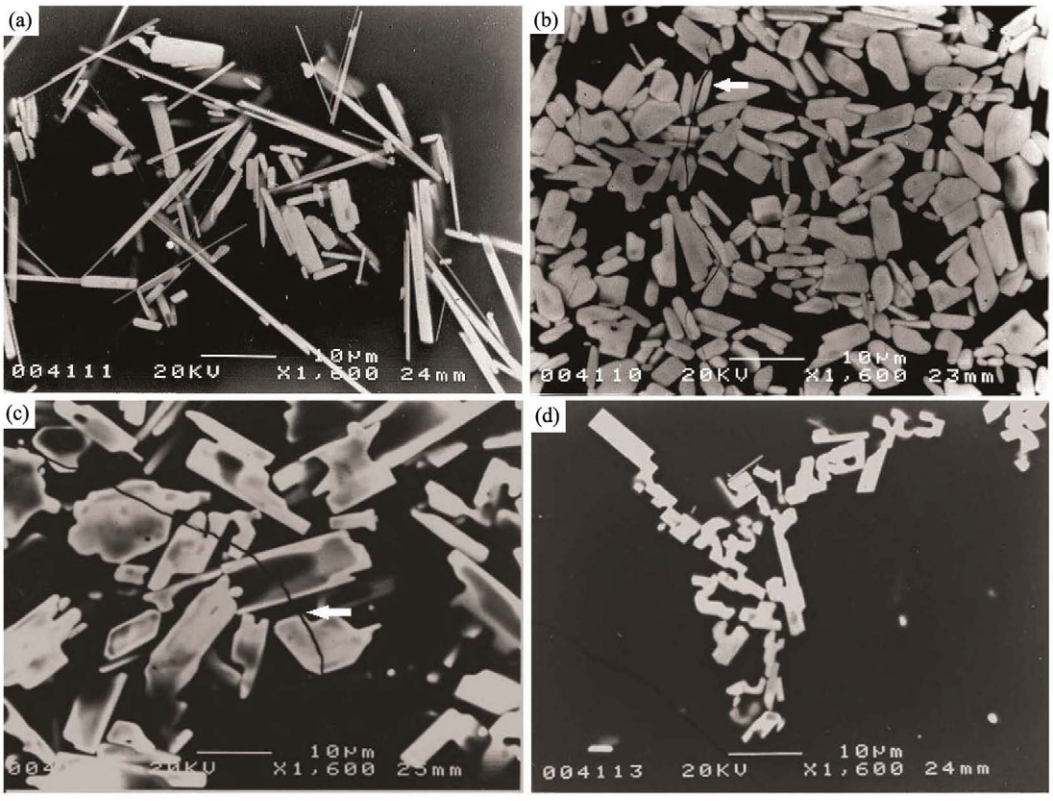

Fig. 8 Scanning electron micrographs of silicon nitride surfaces oxidized for 64 h at 1400 ºC
(a) SN-GH; (b) SN-LH; (c) SN-LCH; (d) SN-LGH

pure La_2O_3, hardness identical to that of the latter, but with microstructure and fracture toughness similar to the samples with Gd_2O_3 additions.

After the HIP process, reduction in number of closed pores resulted in hardness increase. The hardness variation among the sinter-HIPed samples was similar to that observed in samples obtained by conventional sintering, taking into consideration the type and amount of additives. However, there was a marked reduction in the average aspect ratio of β-Si_3N_4 grains, depending on the microstructure before HIP. This reduction was significant in samples with an initial microstructure characterized by grains with high aspect ratio.

The highest oxidation resistance was observed in samples containing Gd_2O_3 (SN-GH and SN-LGH) followed by samples with La_2O_3 concentrate (SN-LCH) and then, pure La_2O_3 (SN-LH). This finding was attributed to the small size of Gd^{3+} cation that could form a viscous amorphous silicate phase in the sinter-HIP ceramics. Furthermore, the small Gd^{3+} cation probably reduced the mobility of the added cations, the former being more stable within the intergranular phase of the ceramic, and thus contributing to the increased oxidation resistance.

Finally, the morphology of the crystals formed on the oxidized layer depends also on the initial composition of the ceramic, although no significant differences were noted in the phases present after the oxidation process.

References:

[1] Swain M V. Structural and Properties of Ceramics. New York: VCH Publishers, 1994 (Materials Science and Technology. 11).

[2] Hampshire S. Engineering properties of nitrides. Edited by Schneider. Los Angeles: ASM International, 1991. 813.

[3] Ziegler G, Heinrich J, Wötting G. Review-relationships between processing, microstructure and properties of dense and reaction-bonded silicon nitride. *J. Mater. Sci.*, 1987, **22**: 3041.

[4] Goto Y, Thomas G. Microstructure of silicon nitride ceramics sintered with rare-earth oxides. *Acta Metall. Mater.*, 1995, **43**: 923.

[5] Ling G, Yang H. Pressureless sintering of silicon nitride with magnesia and yttria. *Mater. Chem. Phys.*, 2005, **90**: 31.

[6] Lu H H, Huang J L. Effect of Y_2O_3 and Yb_2O_3 on the microstructure and mechanical properties of silicon nitride ceramics. *Ceram. Int*., 2001, **27**: 621.

[7] Sanders W A, Mieskowski D M. Strength and microstructure of sintered Si_3N_4 with rare-earth-oxide additions. *Am. Ceram. Soc. Bull*., 1985, **64**: 304.

[8] Choi H J, Lee J-G, Kim Y-W. High temperature strength and oxidation behaviour of hot pressed silicon nitride-disilicate ceramics. *J. Mater. Sci*., 1997, **32**: 282.

[9] Hong Z L, Yoshida H, Ikuhara Y, Sakuma T, Nishimura T, Mitomo M. The effect of additives on sintering behaviour and strength retention in silicon nitride with RE-disilicate. *J. Eur. Ceram. Soc*., 2002, **22**: 527.

[10] Anstis G R, Chantikul P, Lawn B R, Marshall D B. A critical evaluation of indentation techniques for measuring fracture toughness; I, Direct crack measurements. *J. Am. Ceram. Soc.*, 1981, **64**: 533.

[11] Miyazaki H, Hyuga H, Yoshizawa Y, Hirao K, Ohji T. Correlation of wear behavior and indentation fracture resistance in silicon nitride ceramics hot-pressed with alumina and yttria. *J. Eur. Ceram. Soc*., 2009, **29**: 1535.

[12] Tatarko P, Lojanová S, Dusza J, Sajgalik P. Influence of various rare-earth oxide additives on microstructure and mechanical properties of silicon nitride based nanocomposites. *Mater. Sci. Eng.*, 2010 A, **527**: 4771.

[13] Greskovich C, Yeh H C. Hardness of dense β-Si_3N_4. *J. Mater. Sci. Lett*., 1983, **2**: 657.

[14] MacKenzie K J D, Shimada S S, Aoki T. Thermal oxidation of carbothermal SiAlON powder: reaction sequence and kinetics. *J. Mater. Chem.*, 1997, **7**: 527.

[15] MacKenzie K J D, Sheppard C M, Barris G C, Mills A M, Shimada S, Kiyono H. Kinetics and mechanism of thermal oxidation of SiAlON ceramic powders. *Thermochim. Acta*, 1998, **318**: 91.

[16] Pomeroy M, Hamsphire S. Oxidation processes in silicon-nitride-based ceramics. *Mater. Sci. Eng*., *A*, 1989, **109**: 389.

[17] Pan X. Atomistic structure of silicon nitride / silicate glass interfaces. *J. Am. Ceram. Soc.* 1996, **79**: 2975.

[18] Echeberria J, Castro F. Oxidation of silicon nitride sintered with ceria and alumina. *Mater. Sci. Technol*., 1990, **6**: 497.

[19] Monteverde F, Bellosi A. High oxidation resistance of hot pressed silicon nitride containing yttria and lanthania. *J. Eur. Ceram. Soc.*, 1998, **18**: 2313.

[20] Smolin B Y I, Shepelev Y F. The crystal structures of the rare-earth pyrosilicate. *Acta Cryst.*, 1970, **B26**: 484.